Journal of Statistical Mechanics: Theory and Experiment
An IOP and SISSA journal

PAPER: Classical statistical mechanics, equilibrium and non-equilibrium

Percolation and jamming properties in object growth model on a lattice with impurities

D Dujak[1], A Karač[2], Lj Budinski-Petković[3], Z M Jakšić[4] and S B Vrhovac[4,*]

[1] Faculty of Electrical Engineering, University of Sarajevo, Sarajevo 71000, Bosnia and Herzegovina
[2] Polytechnic Faculty, University of Zenica, Zenica, Bosnia and Herzegovina
[3] Faculty of Engineering, University of Novi Sad, Trg D. Obradovića 6, Novi Sad 21000, Serbia
[4] Institute of Physics Belgrade, University of Belgrade, Pregrevica 118, Zemun 11080, Belgrade, Serbia
E-mail: vrhovac@ipb.ac.rs

Received 1 October 2022
Accepted for publication 16 January 2023
Published 16 February 2023

Online at stacks.iop.org/JSTAT/2023/023204
https://doi.org/10.1088/1742-5468/acb7d8

Abstract. Percolation model with nucleation and object growth is studied by Monte Carlo simulations on a triangular lattice with point-like impurities. Growing objects are needle-like objects and self-avoiding random walk chains. In each run through the system the lattice is initially randomly occupied by point-like impurities at given concentration ρ_{imp}. Then the seeds for the object growth are randomly distributed at given concentration ρ. The percolation properties and the jamming densities are compared for the two classes of growing objects on the basis of the results obtained for a wide range of densities ρ and ρ_{imp} up to the percolation threshold for the monomer deposition on a triangular lattice. Values of the percolation thresholds θ_p^* have lower values for the needle-like objects than for the self-avoiding random walk chains. The difference is largest for the lowest values of ρ and ρ_{imp}, and ceases near the values of the site percolation threshold for monomers on the triangular lattice, $\rho_p^* \simeq 0.5$. Values of the jamming coverage

*Author to whom any correspondence should be addressed.

1742-5468/23/023204+22$33.00

θ_J decrease with ρ_{imp} for given ρ. This effect is more prominent for the growing random walk chains.

Keywords: percolation, triangular lattice, seeded growth, impurities

Contents

1. Introduction

Understanding and control of cluster growth on solid surfaces is of a great importance in developing nanomaterials with new physical properties. Synthesis of nanoscale building blocks with controlled structure, size, and shape have wide applications in electronics, chemical engineering, medicine, etc. Seeded growth has emerged as a compelling method to create a wide variety of nanocrystal samples [1–6]. Random sequential adsorption (RSA) on a lattice is often used as a basic model for describing these processes [7].

RSA, or irreversible deposition, is a process in which the particles are randomly and sequentially deposited onto a substrate. In the case of the monolayer deposition depositing objects are not allowed to overlap. The adsorbed particles are permanently fixed at their spatial positions. Once an object is placed it affects the geometry of all later placements, so the dominant effect in RSA is the blocking of the available substrate area. The quantity of interest is the coverage θ which is the fraction of the substrate area occupied by the adsorbed particles. The deposition process ceases when no more depositing objects can be placed in any position on the lattice. The system is then jammed in a nonequilibrium disordered state for which the limiting (jamming) coverage θ_J is less than the corresponding density of closest packing [8–11].

During the deposition process the number of deposited objects increases causing the growth of clusters of nearest-neighbor occupied sites. Percolation assumes the existence of a large cluster that reaches two opposite sides of the substrate [12]. Formation of a long-range connectivity in disordered systems attracts a considerable interest thanks to its applications in numerous practical problems such as conductivity in composite

J. Stat. Mech. (2023) 023204

materials, flow through porous media, polymerization, gelation, and even behavior of scale-free random networks such as the Internet [13–21].

In modeling real deposition processes, one often needs to take into account the possibility of defects that interfere the deposition of the particles. The impact of defects on the jamming and percolation in RSA of k-mers on a square lattice was studied in [22–26]. Cornette *et al* [22, 23] investigated numerically both the bond and the site percolation problems for linear k-mers and self-avoiding walks in the presence of impurities. The contaminated lattice was built by randomly selecting a fraction of the elements of the lattice (either bonds or sites) that were considered forbidden for deposition. This research suggested that the concentration of impurities at which percolation becomes impossible decreases rapidly with increasing values of k. Centres and Ramirez-Pastor [24] have investigated the dependence of percolation and jamming thresholds of linear k-mers on the concentration of defects for different values of k, ranging from 2 to 64. They reported that for each fixed value of k, percolation can occur when fraction of imperfect bonds ρ is smaller than the critical concentration of defects. In [25], two models were analyzed—in the first one it was assumed that some fraction of sites was initially occupied by nonconducting point defects, and in the second one that some fraction of the sites in the k-mers was nonconducting. The dependence of the percolation threshold on the length of the k-mers and on the impurity concentration was analyzed. Above some critical concentration of defects, percolation was found to be blocked even at the jamming limit. Tarashevich *et al* [26] have studied the influence of defects on the behavior of electrical conductivity in a monolayer produced by the isotropic and anisotropic deposition of k-mers onto a square lattice. Two kinds of defects were involved into consideration. The defects in the substrate (impurities) prevent deposition of the particles. Additionally, it was supposed that some parts of the k-mers may be either conducting or non-conducting (defective). Calculation of the electrical conductivities gave an explicit confirmation that even a very small concentration of any kinds of defects has a strong impact on the electrical conductivity. Jamming and percolation on a triangular lattice with extended impurities was studied in [27]. For needle-like impurities of various lengths ℓ at various concentrations p, percolation threshold θ_p^* was determined for k-mers, angled objects and triangles of two different sizes. For sufficiently large impurities, percolation threshold θ_p^* of all examined objects was found to increase with the concentration p, and this increase was more prominent for impurities of a larger length ℓ.

Recently, we proposed a model of granular growth, from nucleation to percolation and jamming [28]. This model can be regarded as a very simple picture of the size- and shape-controlled nano-particles growth. Actually, we examine numerically a percolation model with nucleation and simultaneous growth of multiple finite clusters, on a triangular lattice. Growing objects are needle-like objects, random walk chains, and 'wrapping' objects whose size is gradually increased by wrapping the walks in several different ways, making triangles, rhombuses, and hexagons. For the growing needle-like objects and the growing random walk chains, the percolation threshold θ_p^* increases with the seed density ρ for lower values of ρ, reaches a broad maximum, and slightly falls for higher values of the seed density. The growing random walk chains cover the surface more efficiently

J. Stat. Mech. (2023) 023204

than the needle-like objects, and percolation is reached at higher coverages for the growing random walk chains. The percolation threshold is most affected by the way of the object growth at low seed concentrations. This influence ceases when the seed density tends to the percolation threshold for monomers.

Here we present the results of Monte Carlo simulations of the seed-growth on surfaces with point-like impurities at various concentrations on a triangular lattice. We compare the results for the percolation thresholds and jamming coverages for growing needle-like objects and growing random walk chains. To gain a better insight into the structure of the jammed state, we consider the size distribution of deposited growing objects. The main goal of the work is to investigate the way the seed growth and the deposit formation is affected by the presence of impurities.

The paper is organized as follows. Section 2 describes the details of the model and the simulations. Results and discussions are given in section 3, while section 4 contains some additional comments and final remarks.

2. Definition of the model and the simulation method

Simulations of the object growth are performed on a two-dimensional triangular lattice of size L with periodic boundary conditions. In each run through the system the lattice is initially randomly occupied by point-like impurities at given concentration ρ_{imp}, and by the seeds (monomers) for the object growth randomly distributed at given concentration ρ. Concentrations ρ_{imp} and ρ are defined as fractions of the lattice occupied by impurities and seeds, respectively.

The growing objects are needle like shapes (k-mers) of length $\ell = k - 1$, and shapes made by self-avoiding random walk chains. A self-avoiding shape of length ℓ is a sequence of distinct vertices such that each vertex is a nearest neighbour of its predecessor. The chains are formed by self-avoiding random walks with constraints that step $i + 1$ cannot return to the site at step i, and there is no intersection of the walk. At each Monte Carlo step, the length ℓ of k-mers and random walk shains is increased or remains unchanged, according to the rules that will be presented in the following text.

At the beginning of each run point-like impurities are distributed randomly through the RSA process. The impurities are inserted randomly up to the chosen coverage fraction ρ_{imp} less than $\sim$0.5, i.e. less than the percolation threshold for the monomers on the triangular lattice [27]. Then the monomer seeds are deposited also through the RSA model up to the chosen coverage ρ, also less than $\sim$0.5. After the initial configuration is prepared, a random growing process is initiated in the system.

At each Monte Carlo step, a lattice site occupied by a seed is selected at random. Then an unoccupied adjacent site is selected at random according to the rules for the object growth—the needle-like objects or the self-avoiding random walk chains. In the case of needle-like shapes, the chosen k-mer extends in the direction of the first step in the formation of the depositing object. If the corresponding adjacent site is occupied by an impurity or by the previously deposited object, the attempted k-mer elongation is not possible and the object remains unchanged. In the case of random walk chains, the selected chain randomly extends into one of the empty nearest neighbour sites. If all nearest neighbour sites are occupied, the chosen chain does not change.

J. Stat. Mech. (2023) 023204

Growth of the objects lead to the contact of two objects when they are separated by a single lattice spacing. Then they are merged into a single cluster. The coverage of the surface is increased in the process up to the percolation threshold, when a cluster that extends through the whole system appears. Periodic boundary conditions can be applied in two ways for triangular lattices, i.e. twisted (helical) boundary conditions and conventional boundary conditions. Conventional boundary conditions (percolation on a torus) have been used throughout the paper without losing generality, i.e. sites on an open border are connected to corresponding sites on the opposite border. We say that a percolating cluster arises in the system when the opposite borders of the finite lattice are connected via some path of nearest neighbor sites occupied by the particles. The tree-based union and find algorithm was used to determine the percolation threshold [29]. Each cluster of connected sites is stored as a separate tree, having a single 'root' site. All sites in the cluster possess pointers to the root site, so it is simple to ascertain whether two sites are members of the same cluster. When a deposited object connects two separate clusters, they are amalgamated by adding a pointer from the root of the smaller cluster to the root of the larger one. This procedure is repeated until the percolation threshold is reached.

Another quantity of interest is the jamming limit θ_{J}, which is reached when no more depositing objects can be placed in any position on the lattice. In our model this is the coverage fraction at which no more growing object can be increased according to the set rules. Data are averaged over 500 independent runs through the system for each lattice dimension and for each set of the parameters.

3. Results and discussion

Percolation and jamming properties are studied for growing k-mers and growing self-avoiding random walks. Results are obtained for a wide range of impurity concentrations ρ_{imp} and for a wide range of initial monomer (seed) densities ρ.

For percolation-type systems the dependence of the effective percolation threshold θ_p (the mean value of threshold measured for a finite lattice) on the linear size L of the lattice is described correctly by the finite-size scaling theory [12]. The effective percolation threshold θ_p approaches the asymptotic value θ_p^* for $L \to \infty$ via the power law:

$$\theta_p - \theta_p^* \propto L^{-1/\nu}. \tag{1}$$

Here θ_p^* is the exact percolation threshold (as $L \to \infty$), and ν is the correlation length critical exponent. For two-dimensional systems the theoretical value for ν is $\nu = 4/3$. Relationship (1) allows us to extrapolate the percolation threshold for an infinite system. In general, finite-size scaling implies that estimates converge to θ_p^* as $L^{-1/n}$ [12], but for certain symmetric systems, such as a square open boundary for site percolation on a square lattice, the convergence goes as $L^{-1-1/n}$ [29] and even faster for wrapping around a periodic system [30].

Simulations were performed for lattice sizes ranging from $L = 100$ to $L = 3200$. Plotting the obtained value θ_p of the percolation threshold for various lattice sizes against

J. Stat. Mech. (2023) 023204

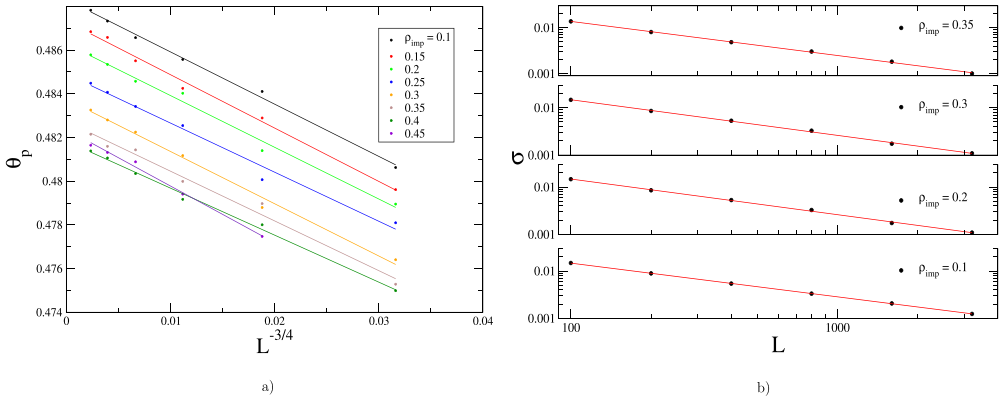

Figure 1. (a) Finite-size scaling of the percolation threshold θ_p against $L^{-1/\nu}$, with $\nu = 4/3$, for growing needle-like objects ($k-$mers) for various values impurity concentrations ρ_{imp} and for initial monomer density $\rho = 0.3$. (b) Standard deviations σ of the percolation threshold on double logarithmic scale for growing k-mers and various values of impurity concentrations ρ_{imp} in the case of seed density $\rho = 0.3$. Straight lines correspond to the best fit according to the power law of equation (2) with the exponents 0.711 ± 0.003, 0.753 ± 0.015, 0.752 ± 0.015, and 0.742 ± 0.012 for impurity concentrations $\rho_{\text{imp}} = 0.1$, 0.2, 0.3, 0.35, respectively.

$L^{-1/\nu}$, confirms the validity of the finite-size scaling in the system and determines the asymptotic value of the percolation threshold θ_p^*. Finite-size scaling of the percolation threshold θ_p for the growing needle-like objects is illustrated in figure 1(a) for various impurity concentrations ρ_{imp} and for initial monomer density $\rho = 0.3$.

According to the scaling theory the standard deviation σ of the percolation threshold measured for a finite lattice L satisfies the power law:

$$\sigma \propto L^{-1/\nu}. \tag{2}$$

In figure 1(b), the standard deviation σ vs L is shown on a double logarithmic scale for the growing k-mers and initial monomer density $\rho = 0.3$. For all impurity densities ρ_{imp} we obtained the confirmation of the power law of equation (2) with the value of the exponent $1/\nu$ ranging from 0.710 to 0.755. These results are in a good agreement with the universal value $1/\nu = 3/4$ for 2D percolations.

At low impurity concentrations it is easier to make connections between the growing objects, and relatively low values of the seed densities are enough to achieve percolation. For high impurity concentrations higher seed densities are needed for reaching the percolation threshold. The interplay between the seed density and the density of impurities is illustrated in figure 2(a). This figure shows the minimum seed densities required to achieve the percolation transition for a given value of the impurity density. Values of the corresponding percolation thresholds are shown in figure 2(b) as a function of the impurity concentration and in figure 2(c) as a function of the seed density.

Dependence of the percolation threshold on the initial seed density for various impurity concentrations is shown for the growing needle-like objects in figure 3. At lower values of the initial seed density ρ, θ_p^* grows monotonically for all impurity concentrations. At

J. Stat. Mech. (2023) 023204

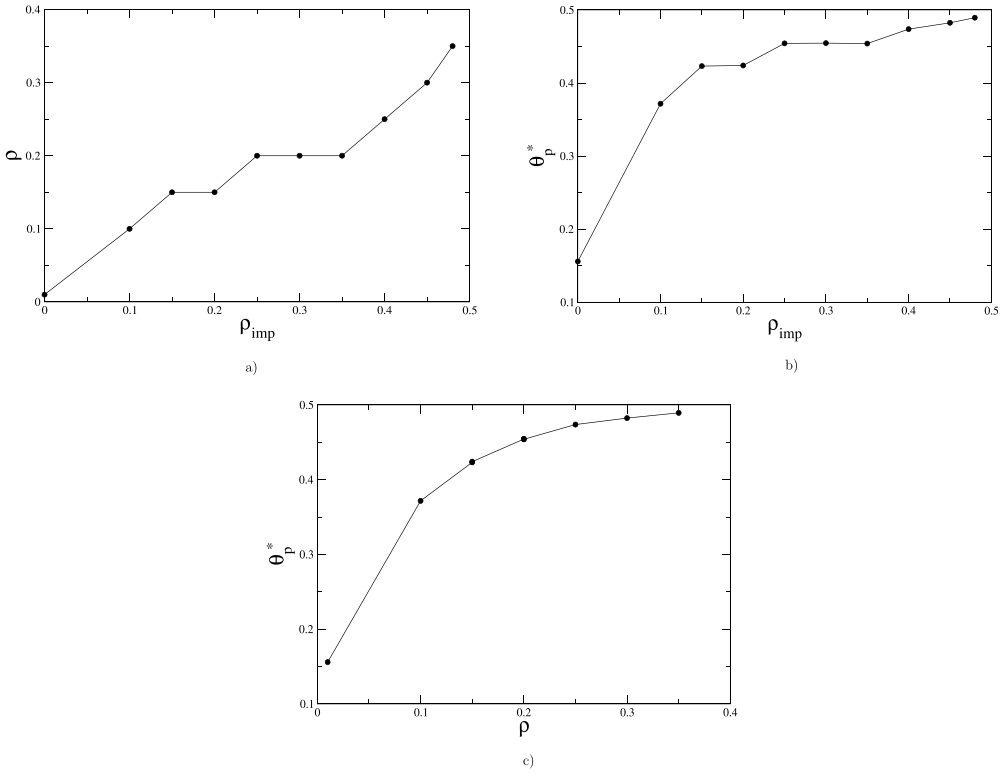

Figure 2. (a) Interplay between the seed density ρ and the density of impurities ρ_{imp} in the case of growing needle-like objects. At low impurity concentrations relatively low values of seed densities are enough to achieve percolation. For higher impurity concentrations higher seed densities are needed for reaching the percolation threshold. (b) Corresponding values of the percolation threshold θ_p^* vs the impurity concentration ρ_{imp}. (c) Corresponding values of the percolation threshold θ_p^* vs the seed density ρ.

low values of the initial seed densities objects have enough space to grow, surface is porous, and the percolation threshold is reached at low values of the coverage. As the seed density increases, the contribution of small objects to the coverage increases and the percolation threshold θ_p^* is reached at higher coverages. Except for the highest impurity concentrations, close to the percolation threshold, the percolation threshold reaches a broad maximum for higher initial seed densities, and slightly falls for larger ρ, as shown in the inset of figure 3.

In figure 4 dependence of the percolation threshold on the impurity concentration for the growing needle-like objects is shown for various initial seed densities. At low values of the initial seed densities, percolation threshold can be reached only for low values of the impurity concentration. Value of ρ_{imp} at which the percolation can be reached increases with the growth of ρ. Values of the percolation threshold θ_p^* for various values of the initial seed density ρ and impurity concentration ρ_{imp} shown in figures 3 and 4 for growing needle-like objects are also given in table 1 (see the appendix).

Values of the jamming coverage θ_{J} for the growing needle-like objects are shown in figure 5 as a function of the initial seed density ρ for various impurity concentrations

J. Stat. Mech. (2023) 023204

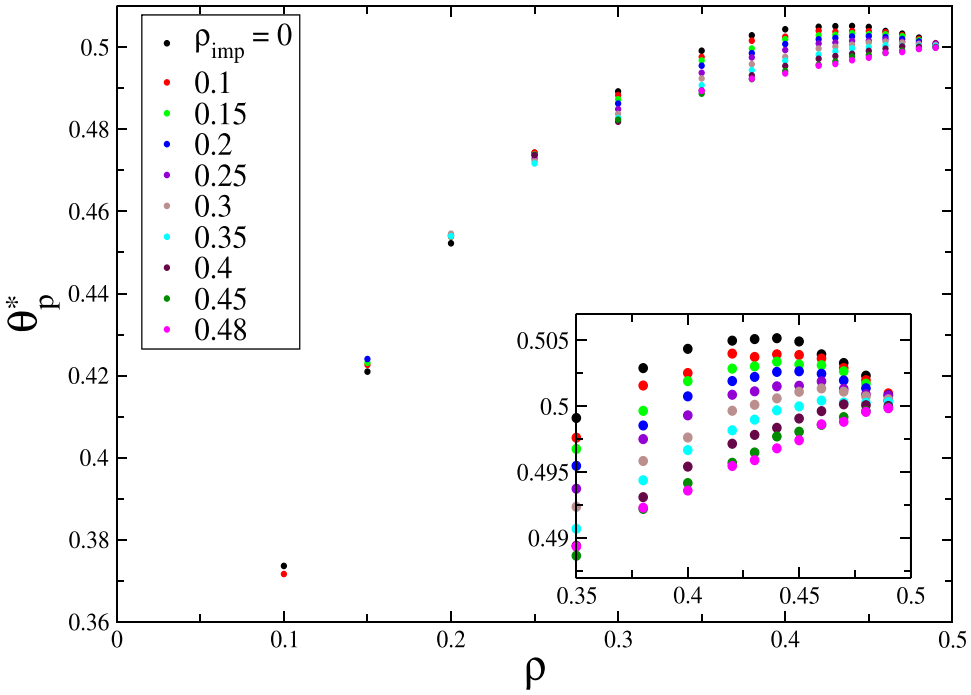

Figure 3. Dependence of the percolation threshold θ_p^* on the initial seed density ρ for growing needle-like objects. Results are shown for various impurity concentrations ρ_{imp} given in the legend. The inset shows the enlarged part of this graph that displays a non-monotonic behavior.

ρ_{imp}. It can be seen that θ_{J} monotonically grows with ρ for all impurity concentrations. As expected, larger seed density provides growth of more objects, including especially the short ones, covering the surface more efficiently. Jamming coverage θ_{J} vs the impurity concentration ρ_{imp} is presented in figure 6 for various values of the seed densities ρ. For a given ρ, θ_{J} decreases with ρ_{imp}, since larger impurity concentrations leave less space for the growing objects.

In order to gain a better insight into the structure of coverings generated by the process of the object growth, we consider the number of deposited k-mers $N(k)$, normalized by the initial number of seeds N_0. Dependence of the ratio $N(k)/N_0$ on the object length $\ell = k - 1$ for the system in the jamming state is shown in figure 7 for various values of the impurity concentrations ρ_{imp} and various values of the seed densities ρ given in the legend of each figure. At lower impurity concentrations (figure 7(a)), maximum of the ratio $N(k)/N_0$ is for the length equal unity for all seed concentrations, i.e. dimers are the most numerous objects in the deposit at the jamming coverage. For larger impurity concentrations (figures 7(b) and (c)), maximum of the object ratio corresponds to monomers for sufficiently large seed densities.

In figure 8 dependence of the ratio $N(k)/N_0$ on the object length for the system in the jamming state is shown for various values of the seed densities ρ and various values of the impurity concentrations ρ_{imp} given in the legends. It can be seen that at the lower seed densities (figures 8(a) and (b)), dimers are the most numerous objects in the deposit at the jamming coverage for all impurity concentrations. With the increase of the

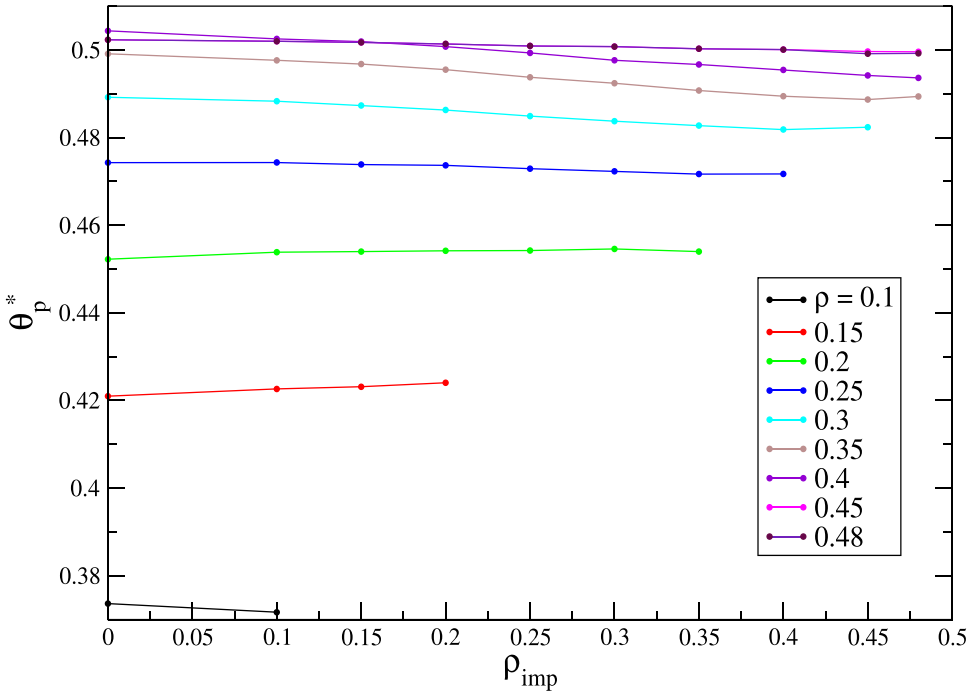

Figure 4. Dependence of the percolation threshold θ_p^* on the impurity concentration ρ_{imp} for growing needle-like objects. Results are shown for various initial seed densities ρ given in the legend.

seed concentrations, monomers prevail at larger values of the impurity concentrations (figure 8(c)). Increase in the seed concentration and the impurity concentration suppress the object growth and the ratio corresponding to monomers increases.

Values of the percolation threshold θ_p^* against $L^{-1/\nu}$, for the growing self-avoiding random walks are shown in figure 9(a) for various values impurity concentrations ρ_{imp} and for initial monomer density $\rho = 0.3$. These graphs also confirm the validity of the finite-size scaling in the system and allow the determination of the asymptotic value of the percolation threshold θ_p^*. Note that, at high impurity concentrations there are difficulties in reaching percolation on smaller lattices for low seed concentrations, but they are less pronounced than in the case of k-mers.

In figure 9(b) the standard deviation σ vs L is shown on a double logarithmic scale for the growing self-avoiding random walks for various values of the impurity concentrations ρ_{imp} and for initial monomer density $\rho = 0.3$. For all impurity concentrations and seed densities we obtained the confirmation of the power law of equation (2) with the value of the exponent $1/\nu$ ranging from 0.731 to 0.746.

Dependence of the percolation threshold θ_p^* on the seed concentration ρ for growing random walk chains are shown in figure 10 for various impurity concentrations ρ_{imp} given in the legend. Similarly as for the needle-like objects, θ_p^* grows monotonically at lower values of the initial seed density ρ. Except for the impurity concentrations close to the percolation threshold for monomers, the percolation threshold for growing self-avoiding random walk chains reaches a broad maximum for high initial seed densities.

J. Stat. Mech. (2023) 023204

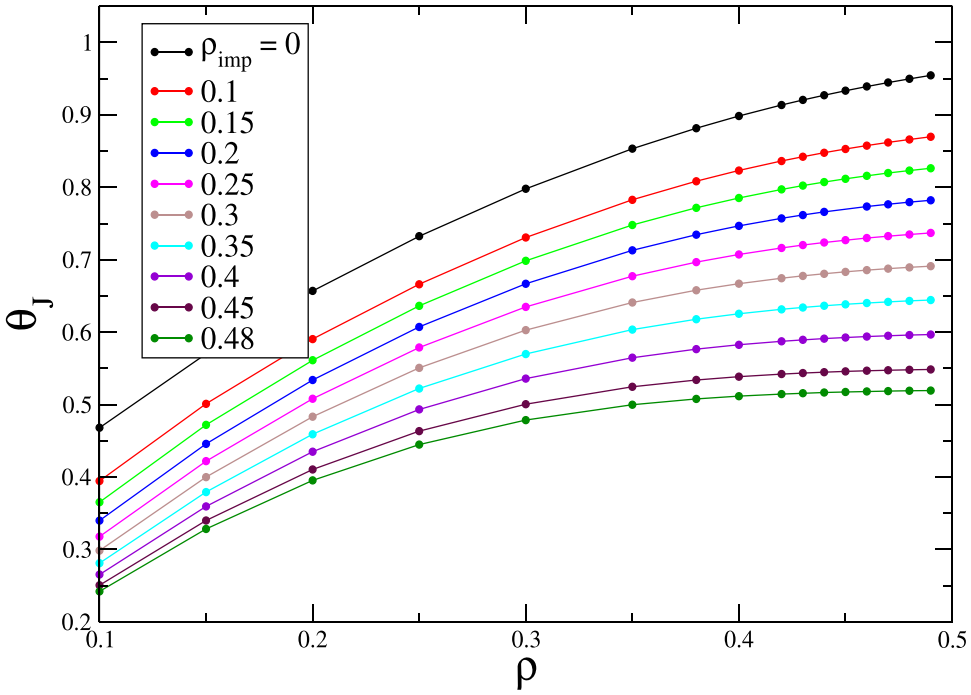

Figure 5. Jamming coverage θ_J for growing needle-like objects (k-mers) vs the initial seed density ρ for various impurity concentrations ρ_{imp} given in the legend.

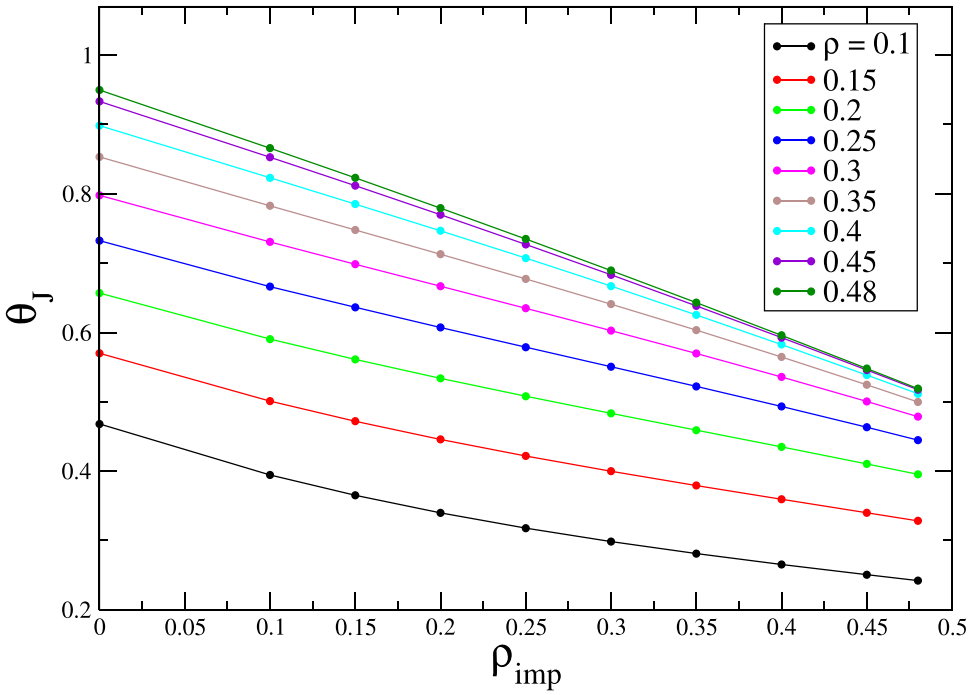

Figure 6. Jamming coverage θ_J for growing needle-like objects (k-mers) vs the density of impurities ρ_{imp} for various initial seed densities ρ given in the legend.

J. Stat. Mech. (2023) 023204

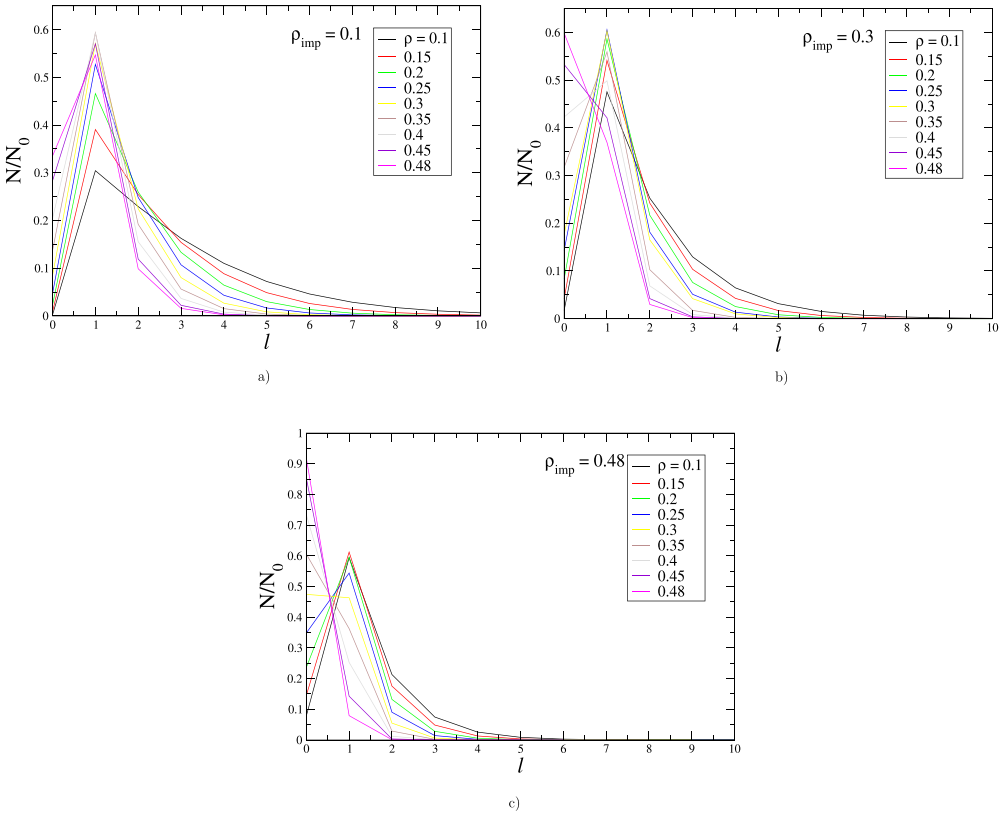

Figure 7. Dependence of the normalized number of deposited k-mers $N(k)/N_0$ on the object length $\ell = k - 1$ for the system in the jamming state for: (a) $\rho_{\text{imp}} = 0.1$; (b) $\rho_{\text{imp}} = 0.3$; (c) $\rho_{\text{imp}} = 0.48$. Results are given for various values of the seed densities ρ that are indicated in the legend. Here, N_0 is the initial number of seeds at a given seed density ρ.

Figures 3 and 10 show that for sufficiently low impurity concentrations ρ_{imp}, the dependence of the percolation threshold θ_p^* on the seed density ρ is non-monotonic. First, we will explain the existence of a broad maximum in the dependence of the percolation threshold θ_p^* on the seed density ρ in cases of low concentrations of impurities. Namely, during the increase of seed (monomer) density from $\rho = 0$ to $\rho = 0.5$, all curves must finish at the same point, $\theta_p^* = 0.5$, which corresponds to the percolation threshold for monomers. However, for sufficiently high seed densities, the percolation threshold reaches values higher than 0.5. In that case, dimers are the dominant component of the deposit (see, for example, figure 7). Then short objects can grow from monomers (seeds) in sufficient numbers so the lattice coverage can become greater than 0.5 without the percolation transition occurring. In fact, the seed distribution reduces the connectivity of clusters on the lattice and thereby increases the percolation threshold above 0.5. However, lattice filling above a density of 0.5 does not occur when the impurity density is very high because the growth of objects is then significantly prevented.

J. Stat. Mech. (2023) 023204

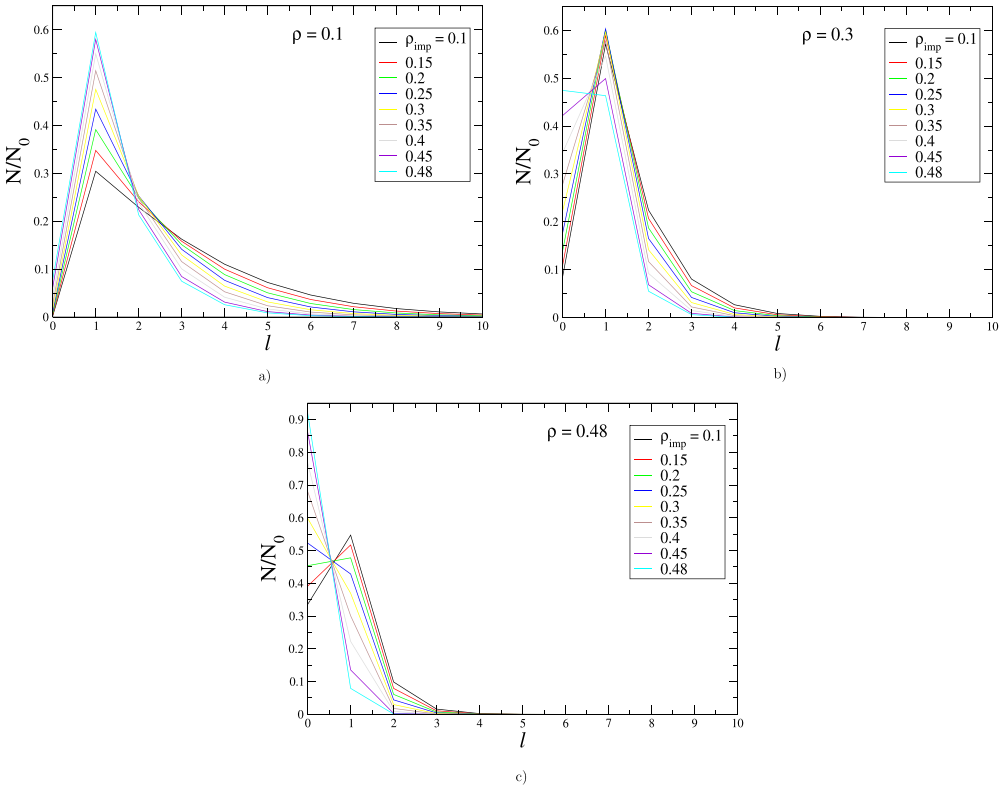

Figure 8. Dependence of the normalized number of deposited k-mers $N(k)/N_0$ on the object length $\ell = k-1$ for the system in the jamming state for initial seed densities: (a) $\rho = 0.1$; (b) $\rho = 0.3$; (c) $\rho = 0.48$. Results are given for various values of the impurity concentrations ρ_{imp} that are indicated in the legend. Here, N_0 is the initial number of seeds at a given seed density ρ.

Dependence of θ_p^* on the impurity concentration for the growing random walk chains is shown in figure 11 for various seed concentrations given in the legend. For a given seed concentration, θ_p^* decreases with impurity concentration, reaches a minimum and slightly increases for the impurity concentrations close to the percolation threshold for monomers on the triangular lattice ($\sim$0.5). Values of the percolation threshold θ_p^* for various values of the initial seed density ρ and impurity concentration ρ_{imp} shown in figures 10 and 11 for growing random walk chains are also given in table 2 (see the appendix).

Comparison of the influence of the seed density ρ and the impurity concentration ρ_{imp} on the percolation threshold θ_p^* for the growing needle-like objects (circles) and for the growing random walk chains (squares) is given in figure 12. In figure 12(a) dependence of θ_p^* on ρ is shown for three different values of the impurity concentration given in the legend. We can see that the values of θ_p^* have lower values for the needle-like objects than for the self-avoiding random walk chains in the whole seed density range. This difference is more prominent for lower values of impurity concentrations and lower seed

J. Stat. Mech. (2023) 023204

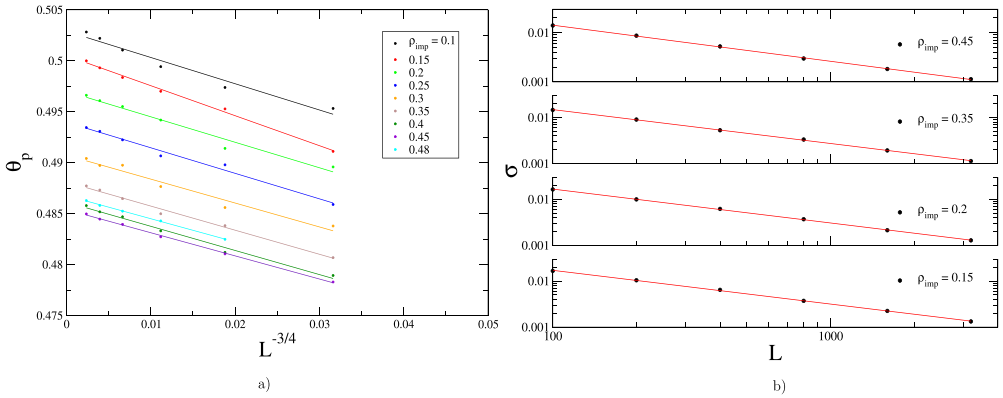

Figure 9. (a) Finite-size scaling of the percolation threshold θ_p against $L^{-1/\nu}$, with $\nu = 4/3$, for the growing random walk chains for various values impurity concentrations ρ_{imp} and for initial monomer density $\rho = 0.3$. (b) Standard deviations σ of the percolation threshold on double logarithmic scale for growing random walk chains and various values of impurity concentrations ρ_{imp} in the case of seed density $\rho = 0.3$. Straight lines correspond to the best fit according to the power law of equation (2) with the exponents 0.734 ± 0.009, 0.745 ± 0.008, 0.746 ± 0.008, and 0.734 ± 0.009 for impurity concentrations $\rho_{\text{imp}} = 0.15$, 0.2, 0.35, 0.45, respectively.

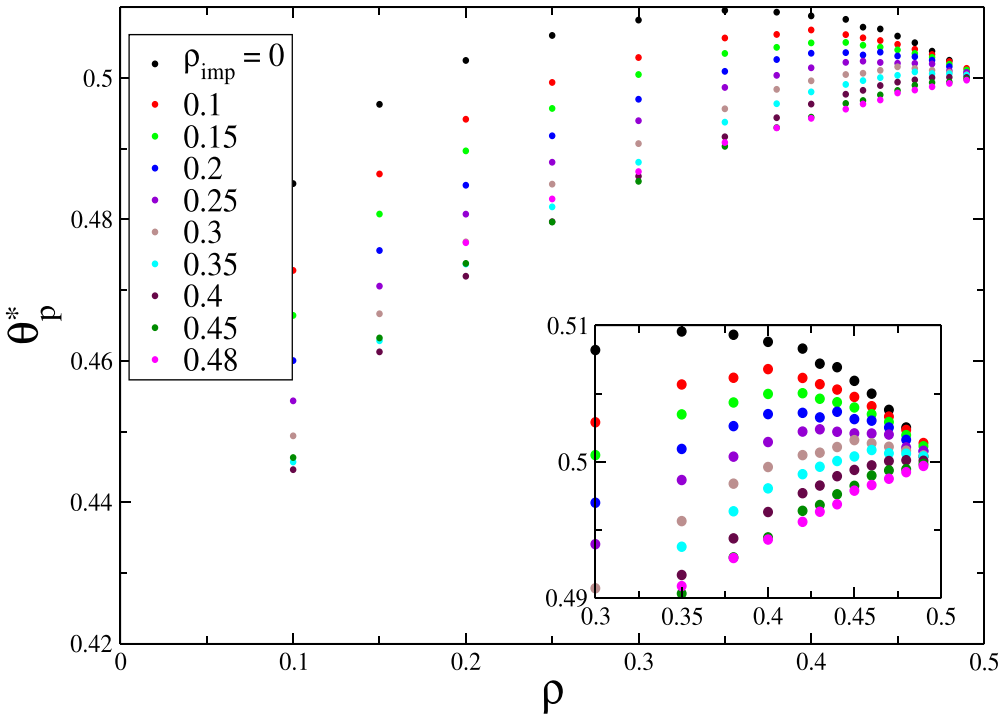

Figure 10. Dependence of the percolation threshold θ_p^* on the initial seed density ρ for growing random walk chains. Results are shown for various impurity concentrations ρ_{imp} given in the legend. The inset shows the enlarged part of this graph that displays a non-monotonic behavior.

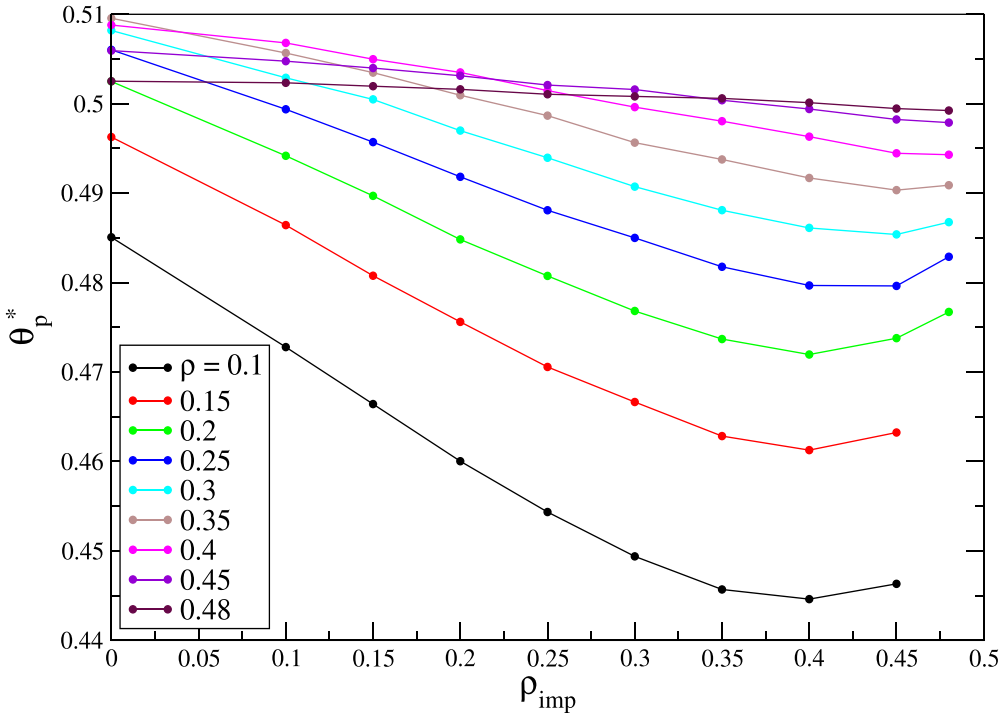

Figure 11. Dependence of the percolation threshold θ_p^* on the impurity concentration ρ_{imp} for the growing random walk chains. Results are shown for various initial seed densities ρ given in the legend.

densities. Surface configuration formed during the object growth is more porous in the case of the needle-like objects and the percolation occurs at lower coverage values. With the growth of the seed density ρ or the impurity density ρ_{imp}, this difference decreases and practically ceases when ρ or ρ_{imp} approach the value of the percolation threshold for monomers on the triangular lattice. In figure 12(b) dependence of θ_p^* on ρ_{imp} is shown for the growing needle-like objects and for the growing random walk chains for three different values of the seed concentration ρ given in the legend. These results also indicate that the values of θ_p^* have lower values for the needle-like objects than for the self-avoiding random walk chains and that the difference is largest for the lowest values of ρ and ρ_{imp}.

Jamming coverage θ_{J} for the growing random walk chains grows with the seed densities for all values of impurity concentrations (figure 13). This growth starts from higher values of θ_{J} than in the case of the growing needle-like objects. At low values of the seed concentrations the growing needle-like objects make porous surface configuration, while the growing random walk chains are more flexible and cover the surface more efficiently. From figure 14, showing the dependence of the jamming coverage θ_{J} for the

J. Stat. Mech. (2023) 023204

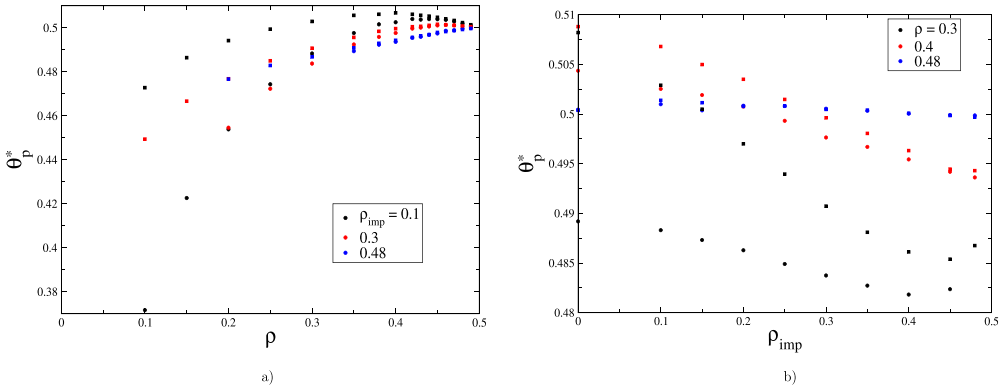

Figure 12. (a) Comparison of the influence of the seed density ρ on the percolation threshold θ_p^* for the growing needle-like objects (circles) and for the growing random walk chains (squares). Dependence of θ_p^* on ρ is shown for three different values of the impurity concentration given in the legend. (b) Comparison of the influence of the impurity concentration $\rho_{\rm imp}$ on the percolation threshold θ_p^* for the growing needle-like objects (circles) and for the growing random walk chains (squares). Dependence of θ_p^* on $\rho_{\rm imp}$ is shown for three different values of the seed concentration given in the legend.

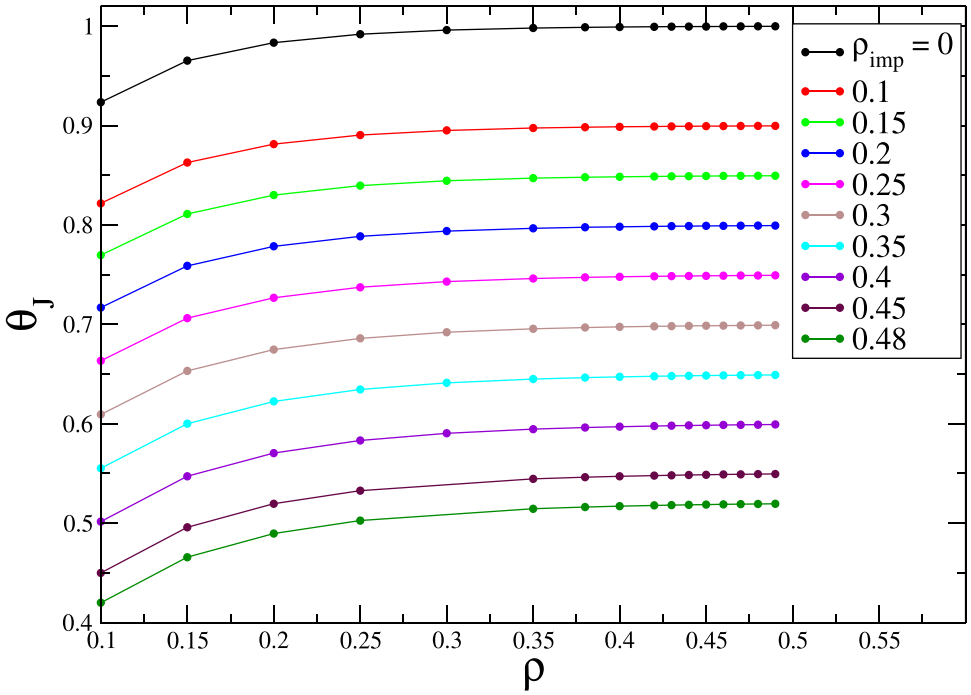

Figure 13. Jamming coverage $\theta_{\rm J}$ for the growing random walk chains vs the initial seed density ρ for various impurity concentrations $\rho_{\rm imp}$ given in the legend.

J. Stat. Mech. (2023) 023204

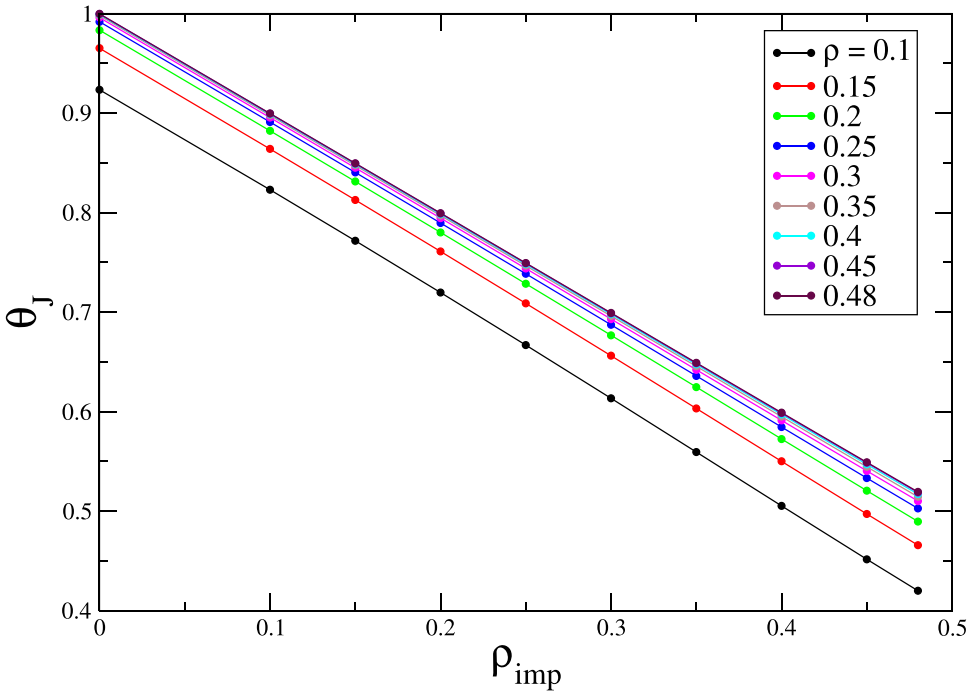

Figure 14. Jamming coverage θ_J for the growing random walk chains vs the density of impurities ρ_{imp} for various initial seed densities ρ given in the legend.

growing random walk chains on the density of impurities ρ_{imp}, it can be seen that the jamming coverage decreases approximately linearly with ρ_{imp}.

Figure 15 shows the normalized number of deposited random walk chains $N(k)/N_0$ as a function of the object length, for various impurity concentrations ρ_{imp} and various initial seed densities ρ given in the legends. In figure 15(a) results for the lowest impurity concentration considered, $\rho_{imp} = 0.1$, are presented. Maximum for the lowest initial seed density $\rho = 0.1$ is for $\ell = 5$, i.e. for a random walk covering six lattice sites. The maximum is shifted towards shorter random walk chains when the seed density increases and for the highest values of ρ, close to the percolation threshold, monomers are the most numerous objects making the deposit. In figures 15(b) and (c) results for $\rho_{imp} = 0.3$ and $\rho_{imp} = 0.48$ are presented, respectively. As the impurity concentration increases, the maximum is shifted towards lower ℓ, and the threshold for the predominance of monomers in the deposit is shifted to lower values of initial seed concentrations. Nevertheless, even for the largest ρ_{imp} considered, there are considerable concentrations of longer objects in the deposit.

Dependence of the normalized number of random walk chains $N(k)/N_0$ on the walk length is presented in figure 16 for various seed concentrations ρ and various impurity

J. Stat. Mech. (2023) 023204

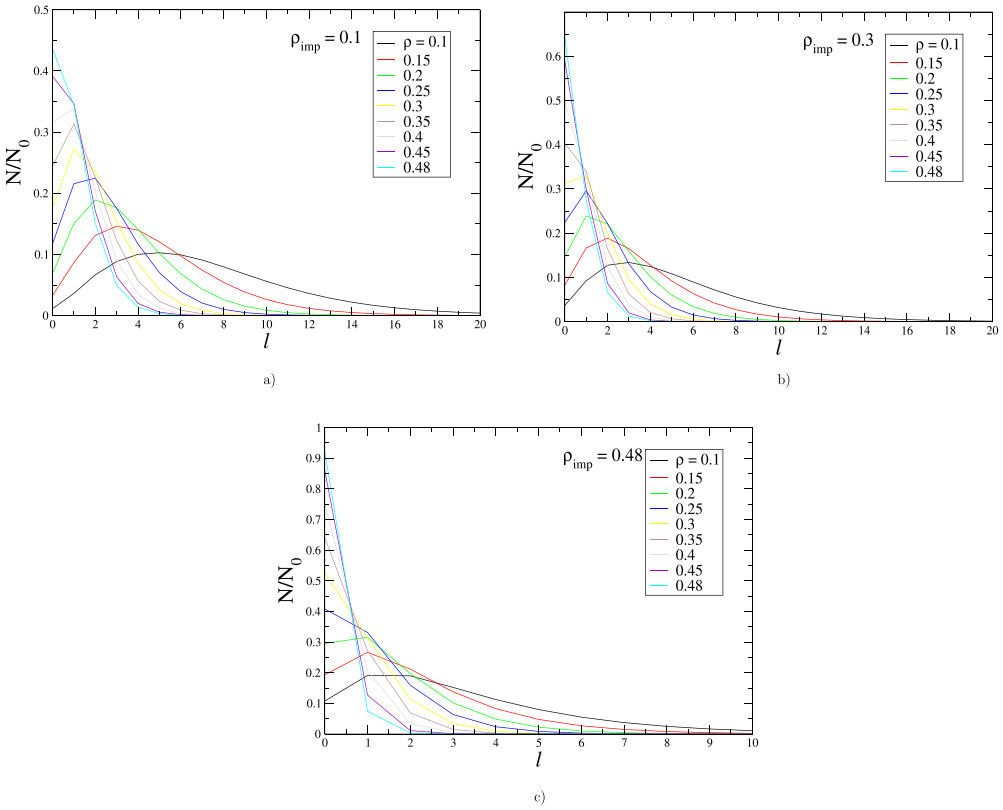

Figure 15. Dependence of the normalized number of deposited random walk chains $N(k)/N_0$ on the chain length $\ell = k - 1$ for the system in the jamming state for: (a) $\rho_{\text{imp}} = 0.1$; (b) $\rho_{\text{imp}} = 0.3$; (c) $\rho_{\text{imp}} = 0.48$. Results are given for various values of the seed density ρ that are indicated in the legend. Here, N_0 is the initial number of seeds at a given density ρ.

concentrations ρ_{imp} given in the legends. For $\rho = 0.1$ and $\rho_{\text{imp}} = 0.1$ the maximum is at $\ell = 5$ (walks covering six lattice sites), and for $\rho = 0.1$ and $\rho_{\text{imp}} = 0.48$ at $\ell = 1$ (walks covering two lattice sites). Increasing the values of ρ and ρ_{imp} causes the shifting of the maximum towards lower values of ℓ. For $\rho = 0.3$ the most numerous objects are dimers only for the sufficiently low impurity concentrations. Further increase of ρ causes shifting of the maximum to the monomers. For the values of ρ close to the percolation threshold for monomers, the most numerous objects in the deposit are monomers for all values of ρ_{imp}. When comparing the structure of the deposit for the growing needle-like objects and the growing random walk chains, the latter form jamming configurations with longer objects. The growing random walk chains are more flexible than the needle-like objects and they can find the path for the growth more easily.

J. Stat. Mech. (2023) 023204

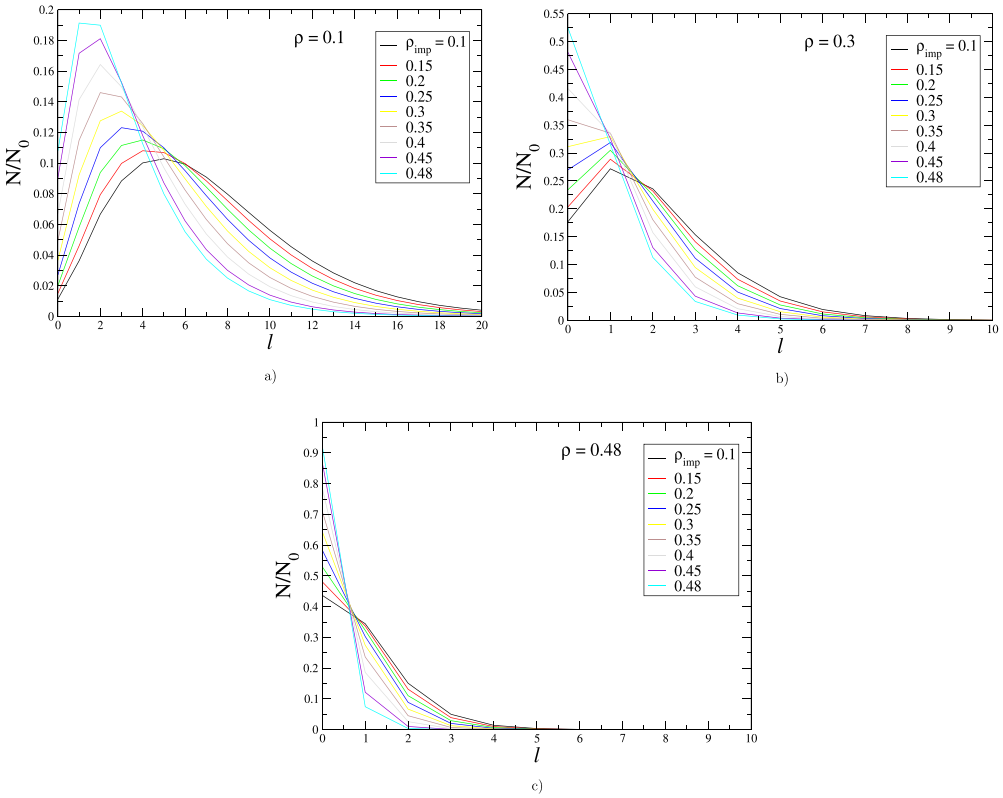

Figure 16. Dependence of the normalized number of deposited random walk chains $N(k)/N_0$ on the chain length $\ell = k - 1$ for the system in the jamming state for: (a) $\rho = 0.1$; (b) $\rho = 0.3$; (c) $\rho = 0.48$. Results are given for various values of the impurity concentrations ρ_{imp} that are indicated in the legend. Here, N_0 is the initial number of seeds at a given seed density ρ.

4. Concluding remarks

Percolation and jamming were studied for growing objects on a triangular lattice with quenched impurities. Growing objects were needle-like shapes and random walk chains and the simulations were performed for various seed concentrations ρ and various impurity concentrations ρ_{imp} up to the percolation threshold for monomer deposition.

The presence of impurities requires higher seed concentrations to achieve percolation during the object growth process on the surface. As a consequence, the percolation threshold increases with the minimum seed density leading to percolation, and also with the corresponding impurity concentration.

In the case of needle-like object growth, at the values of the initial seed densities ρ that are not close to the percolation threshold for the monomers, θ_p^* increases monotonically with the seed density ρ for all impurity concentrations ρ_{imp}. Except for the highest impurity concentrations, close to the percolation threshold, the percolation threshold reaches a broad maximum for high initial seed densities. When results for θ_p^*

https://doi.org/10.1088/1742-5468/acb7d8

J. Stat. Mech. (2023) 023204

are shown vs ρ_{imp} for fixed ρ, the obtained plots show an only slight dependence on ρ_{imp}. Here should be noted that the value of ρ_{imp} at which the percolation can be reached increases with the growth of ρ and hence has an indirect influence on the percolation threshold.

When the growing objects are self-avoiding random walk chains, dependence of θ_p^* on the seed density ρ is similar as in the case of needle-like objects. On the other hand, for a given seed concentration, θ_p^* decreases with impurity concentration, reaches a minimum, and slightly increases for the impurity concentrations close to the percolation threshold for monomers on the triangular lattice. Growing random walk chains are able to avoid the impurities more efficiently than the growing needle-like objects, and the increase of the impurity concentration can decrease the percolation threshold. Comparison of the influence of the seed density ρ and the impurity concentration ρ_{imp} on the percolation threshold θ_p^* for the growing needle-like objects and for the growing random walk chains indicates that the values of θ_p^* have lower values for the needle-like objects than for the self-avoiding random walk chains. The difference is largest for the lowest values of ρ and ρ_{imp}, and ceases near the values of the site percolation threshold for monomers on the triangular lattice, $\rho_p^* \simeq 0.5$.

Values of the jamming coverage θ_{J} for the growing objects increase with the seed concentration ρ for given impurity concentrations ρ_{imp}, and decrease with ρ_{imp} for given ρ. The increase of θ_{J} with ρ is more prominent for the growing needle-like objects, and the decrease of θ_{J} with ρ_{imp} is steeper for the growing random walk chains.

Structure of the jammed state depends on the rules for the object growth, on the initial seed density ρ and on the impurity concentration ρ_{imp}. Comparing the jamming configurations made by the growing needle-like objects and by the growing random walk chains, the latter form jamming configurations with longer objects. The growing random walk chains are more flexible than the needle-like objects and they can form configurations with prevailing longer objects, especially at lower values of the seed densities and the impurity concentrations.

Acknowledgment

This work was supported by the Ministry of Education, Science, and Technological Development of the Republic of Serbia. Numerical simulations were run on the PARADOX supercomputing facility at the Scientific Computing Laboratory of the Institute of Physics Belgrade. We would like to thank the Federal Ministry of Education and Science in Bosnia and Herzegovina for their financial support under Grant No. PtF_EM_IR_06/2021.

Appendix

Values of the percolation threshold θ_p^* for various values of the initial seed density ρ and impurity concentration ρ_{imp} for growing needle-like objects and random walk chains are given in tables 1 and 2, respectively.

J. Stat. Mech. (2023) 023204

Table 1. Values of the percolation threshold θ_p^* for various values of the initial seed density ρ and impurity concentration ρ_{imp} for the growing needle-like objects. The numbers in parentheses are the numerical values of the standard uncertainty of θ_p^* referred to the last digits of the quoted values.

ρ \ ρ_{imp}	0.0	0.1	0.2	0.3	0.4	0.45	0.48
0.1	0.373 64(10)	0.371 67(05)					
0.15	0.420 98(16)	0.422 63(21)	0.424 04(86)				
0.2	0.452 23(34)	0.453 84(23)	0.454 16(11)	0.454 58(26)			
0.25	0.474 28(20)	0.474 31(11)	0.473 66(34)	0.472 29(16)	0.471 70(14)		
0.3	0.489 20(15)	0.488 31(12)	0.486 29(20)	0.483 75(17)	0.481 83(12)	0.482 37(12)	
0.35	0.499 12(31)	0.497 63(11)	0.495 49(19)	0.492 39(25)	0.489 43(11)	0.488 68(12)	0.489 38(19)
0.38	0.502 90(23)	0.501 58(12)	0.498 55(25)	0.495 86(24)	0.493 12(17)	0.492 23(10)	0.492 32(11)
0.4	0.504 36(15)	0.502 53(69)	0.500 76(05)	0.497 64(31)	0.495 43(15)	0.494 19(16)	0.493 62(11)
0.42	0.504 98(17)	0.504 00(13)	0.501 92(13)	0.499 67(08)	0.497 05(12)	0.495 73(33)	0.495 48(13)
0.43	0.505 10(28)	0.503 75(26)	0.502 23(27)	0.500 12(09)	0.497 84(14)	0.496 51(07)	0.495 92(16)
0.44	0.505 17(26)	0.503 95(13)	0.502 61(09)	0.500 61(18)	0.498 37(16)	0.497 72(18)	0.496 82(15)
0.45	0.504 92(11)	0.503 89(09)	0.502 66(12)	0.501 11(07)	0.499 08(11)	0.498 08(10)	0.497 43(10)
0.46	0.503 95(36)	0.503 63(07)	0.502 47(06)	0.501 36(15)	0.499 64(07)	0.498 60(18)	0.498 64(14)
0.47	0.503 29(13)	0.502 91(25)	0.501 97(06)	0.501 12(11)	0.500 15(19)	0.499 19(15)	0.498 83(08)
0.48	0.502 33(08)	0.501 99(16)	0.501 37(20)	0.500 76(12)	0.500 09(08)	0.499 64(07)	0.499 58(05)
0.49	0.500 44(42)	0.500 99(02)	0.500 84(03)	0.500 54(12)	0.500 04(04)	0.499 91(06)	0.499 86(28)

Table 2. Values of the percolation threshold θ_p^* for various values of the initial seed density ρ and impurity concentration ρ_{imp} for the growing random walk chains. The numbers in parentheses are the numerical values of the standard uncertainty of θ_p^* referred to the last digits of the quoted values.

ρ \ ρ_{imp}	0.0	0.1	0.2	0.3	0.4	0.45	0.48
0.1	0.485 07(39)	0.472 79(41)	0.460 03(18)	0.445 69(12)	0.444 61(05)	0.446 32(00)	
0.15	0.496 28(33)	0.486 43(19)	0.475 61(18)	0.462 84(29)	0.461 27(15)	0.463 24(10)	
0.2	0.502 50(27)	0.494 18(21)	0.484 83(14)	0.473 69(08)	0.471 96(18)	0.473 79(54)	0.476 72(12)
0.25	0.506 03(25)	0.499 38(25)	0.491 83(09)	0.481 77(12)	0.479 68(23)	0.479 63(12)	0.482 89(39)
0.3	0.508 20(52)	0.502 90(40)	0.497 00(34)	0.488 10(18)	0.486 12(20)	0.485 39(07)	0.486 76(04)
0.35	0.509 56(22)	0.505 67(24)	0.500 95(05)	0.493 77(07)	0.491 70(10)	0.490 34(11)	0.490 89(11)
0.38	0.509 42(16)	0.506 17(17)	0.502 62(17)	0.496 37(22)	0.494 39(16)	0.492 99(12)	0.492 95(12)
0.4	0.508 80(17)	0.506 80(37)	0.503 50(24)	0.498 05(07)	0.496 32(15)	0.494 46(23)	0.494 30(11)
0.42	0.508 31(18)	0.506 15(11)	0.503 59(17)	0.4999(08)	0.497 70(10)	0.496 41(05)	0.495 60(07)
0.43	0.507 20(41)	0.505 69(08)	0.503 26(14)	0.499 64(08)	0.498 26(12)	0.496 83(16)	0.496 34(04)
0.44	0.506 94(38)	0.505 30(11)	0.503 67(15)	0.500 06(12)	0.498 95(13)	0.497 62(12)	0.496 89(08)
0.45	0.505 94(10)	0.504 76(12)	0.503 13(14)	0.500 39(14)	0.499 41(09)	0.498 24(18)	0.497 89(17)
0.46	0.505 00(09)	0.504 08(07)	0.503 02(13)	0.500 87(24)	0.499 74(08)	0.498 99(13)	0.498 30(06)
0.47	0.503 81(20)	0.503 32(15)	0.502 52(09)	0.500 63(14)	0.500 06(14)	0.499 37(13)	0.498 76(13)
0.48	0.502 52(26)	0.502 34(15)	0.501 61(13)	0.500 60(13)	0.500 12(17)	0.499 46(15)	0.499 24(10)
0.49	0.500 38(42)	0.501 38(02)	0.500 77(10)	0.500 40(05)	0.500 08(03)	0.499 85(05)	0.499 70(32)

J. Stat. Mech. (2023) 023204

References

[1] Nikoobakht B and El-Sayed M A 2003 Preparation and growth mechanism of gold nanorods (NRs) using seed-mediated growth method *Chem. Mater.* **15** 1957–62

[2] Gole A and Murphy C J 2004 Seed-mediated synthesis of gold nanorods: role of the size and nature of the seed *Chem. Mater.* **16** 3633–40

[3] Habas S E, Lee H, Radmilović V, Somorjai G A and Yang P 2007 Shaping binary metal nanocrystals through epitaxial seeded growth *Nat. Mater.* **6** 692–7

[4] Einax M, Dieterich W and Maass P 2013 Colloquium: cluster growth on surfaces: densities, size distributions and morphologies *Rev. Mod. Phys.* **85** 921

[5] Lohse S E and Murphy C J 2013 The quest for shape control: a history of gold nanorod synthesis *Chem. Mater.* **25** 1250–61

[6] Roy B and Santra S B 2017 First-order transition in a percolation model with nucleation and preferential growth *Phys. Rev.* E **95** 010101

[7] Evans J W 1993 Random and cooperative sequential adsorption *Rev. Mod. Phys.* **65** 1281–329

[8] Manna S S and Svrakic N M 1991 Random sequential adsorption: line segments on the square lattice *J. Phys. A: Math. Gen.* **24** L671

[9] Talbot J, Tajrus G, Van Tassel P R and Viot P 2000 From car parking to protein adsorption: an overview of sequential adsorption process *Colloids Surf.* A **165** 287–324

[10] Budinski-Petković L, Vrhovac S B and Lončarević I 2008 Random sequential adsorption of polydisperse mixtures on discrete substrates *Phys. Rev.* E **78** 061603

[11] Budinski-Petković L, Lončarević I, Dujak D, Karač A, Šćepanović J R, Jakšić Z M and Vrhovac S B 2017 Particle morphology effects in random sequential adsorption *Phys. Rev.* E **95** 022114

[12] Staufer D and Aharony A 1994 *Introduction to Percolation Theory* (London: Taylor and Francis)

[13] Kondrat G and Pekalski A 2001 Percolation and jamming in random sequential adsorption of linear segments on a square lattice *Phys. Rev.* E **63** 051108

[14] Kondrat G 2002 Influence of temperature on percolation in a simple model of flexible chains adsorption *J. Chem. Phys.* **117** 6662

[15] Kondrat G 2008 Impact of composition of extended objects on percolation on a lattice *Phys. Rev.* E **78** 011101

[16] Ziff R M 2009 Explosive growth in biased dynamic percolation on two-dimensional regular lattice networks *Phys. Rev. Lett.* **103** 045701

[17] Tsakiris N, Maragakis M, Kosmidis K and Argyrakis P 2010 Percolation of randomly distributed growing clusters: finite-size scaling and critical exponents for the square lattice *Phys. Rev.* E **82** 041108

[18] Ioselevich A S and Kornyshev A A 2002 Approximate symmetry laws for percolation in complex systems: percolation in polydisperse composites *Phys. Rev.* E **65** 021301

[19] Tarasevich Y Y, Lebovka N I and Laptev V V 2012 Percolation of linear k-mers on a square lattice: from isotropic through partially ordered to completely aligned states *Phys. Rev.* E **86** 061116

[20] Budinski-Petković L, Lončarević I, Petković M, Jakšić Z M and Vrhovac S B 2012 Percolation in random sequential adsorption of extended objects on a triangular lattice *Phys. Rev.* E **85** 061117

[21] Cohen R, Erez K, Avraham D B and Havlin S 2001 Breakdown of the internet under intentional attack *Phys. Rev. Lett.* **86** 3682–5

[22] Cornette V, Ramirez-Pastor A J and Nieto F 2006 Percolation of polyatomic species on site diluted lattices *Phys. Lett.* A **353** 452–8

[23] Cornette V, Ramirez-Pastor A J and Nieto F 2006 Percolation of polyatomic species with the presence of impurities *J. Chem. Phys.* **125** 204702

[24] Centres P M and Ramirez-Pastor A J 2015 Percolation and jamming in random sequential adsorption of linear k-mers on square lattices with the presence of impurities *J. Stat. Mech.* **2015** 10011

[25] Tarasevich Y Y, Laptev V V, Vygornitskii N V and Lebovka N I 2015 Impact of defects on percolation in random sequential adsorption of linear k-mers on square lattices *Phys. Rev.* E **91** 012109

[26] Tarasevich Y Y, Laptev V V, Goltseva V A and Lebovka N I 2017 Influence of defects on the effective electrical conductivity of a monolayer produced by random sequential adsorption of linear k-mers onto a square lattice *Physica* A **477** 195–203

[27] Lončarević I, Budinski-Petković L, Dujak D, Karač A, Jakšić Z M and Vrhovac S B 2017 The study of percolation with the presence of extended impurities *J. Stat. Mech.* 2017 093202

J. Stat. Mech. (2023) 023204

[28] Dujak D, Karač A, Jakšić Z M, Budinski-Petković L and Vrhovac S B 2022 Percolation and jamming properties in particle shape controlled seeded growth model *Eur. Phys. J.* B **95** 143
[29] Ziff R M and Newman M E J 2002 Convergence of threshold estimates for two-dimensional percolation *Phys. Rev.* E **66** 016129
[30] Newman M E J and Ziff R M 2001 Fast Monte Carlo algorithm for site or bond percolation *Phys. Rev.* E **64** 016706

J. Stat. Mech. (2023) 023204